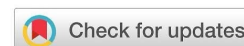# Effect of the magnetic field and exhaust gas recirculation on the performance and emissions of biodiesel engine coated with nanoceramics

Check for updates

Qusai A. Mahdi*, Mahmoud A. Mashkour [ID], Ibtihal A. Mahmoud

Mechanical Engineering Dept., University of Technology-Iraq, Alsina'a street, 10066 Baghdad, Iraq.
*Corresponding author Email: qam.me782000@gmail.com

HIGHLIGHTS

- 10% WCO and 10% EGR with magnetic fields increased LHR C.I. engine brake thermal efficiency by 20%.
- The combined impact decreased BSFC by 18.1%, increased coated engine exhaust temperature by 25% at 100% load, and lowered CO emissions at higher loads
- A 0.5 mm ceramic coating on the engine increased diesel engine exhaust gas temperature by 25%.
- adiabatic engine emits more CO_2 at all load levels, with a18.9% increase at 75% of full load .

ARTICLE INFO

ABSTRACT

This study investigates the influence of ceramic coating on diesel engine efficiency through comprehensive analysis. The investigation was conducted on a four-stroke Kirloskar TV1 diesel engine. The study further examined the effects of employing an 8000 Gauss magnetic field and exhaust gas recirculation on engine performance. The surfaces of the head of the cylinder, the piston, and both the inlet and exhaust valves are then covered with nano-ceramic materials. Atmospheric plasma spray-created nanostructured thermal barrier coatings (TBCs). The feeding powder type is 7% Y_2O_3-ZrO_2 with a particle size of less than 100 nm yttria stabilized zirconia (YSZ) nano X (S4007) ceramic surface coating (350 µm). Bond powder (NiCrAlY) Amdry 962, ranging from 56 to 106µm, has been utilized as a metal bonding coat (150 µm). The results show that the temperature of engine exhaust rises after coating, resulting in a decrease in fuel consumption by 14.22 %. The effect of biofuels on the performance of a compression ignition engine running on diesel fuel was examined. The testing findings revealed that brake thermal efficiency (BTE) improved by 20.5%, and brake-specific fuel consumption (BSFC) decreased by 18.1%. When the load goes up from 50 to 100 percent, however, 38.8 percent and fewer CO percent are observed for the B10+10EGR+8000 Gauss and 0.5 mm coated engine. Also, acceptable increases in emissions were observed in CO_2 levels. Diesel and the B10+EGR10+8000 Gauss un-treatment engine's NOx emission values rise by 49.15 percent and 45 percent, respectively, after the load goes up 75 percent.

1. Introduction

In a combustion engine, the power generated by the combustion will be used for output work; some power is lost through carrying by the cooling system (oil and water), and heat is lost through exhaust. Only one-third of the available power is believed to be turned into meaningful output. Through decreasing heat transfer rates, a low heat rejected (LHR) engine indicates the ability to produce more useful work by transforming unavailable energy. Hence, the engine's efficiency will be increased. Thermal barrier coating was developed to reduce the heat transfer rate and improve overall I.C. engine performance. The application of LHR technology on all main components of the combustion chamber permits proper combustion to occur even when using low-property fuels since the surface temperature of the coating elements is substantially greater than the temperature of the untreated components with the help of combined magnetic field conditioner (MFC), and exhaust gas recirculation (EGR), leading to raising the brake thermal efficiency to high levels, especially when using biofuel. Nowadays, biodiesel has been the most popular substitute for conventional diesel Dhinesh et al. [1], Demirbas [2].

Thermal barrier coatings can last long in applications with constant exposure to thermal stresses resulting from high temperatures, such as gas turbines and internal combustion engines. Saravanan et al. [3] investigated the effects of engine injection pressure, injection time, and EGR on engine pollutant reduction, tested on engines fueled with crude rice bran oil methyl ester. Taguchi's L9 orthogonal array was used to execute the testing. It was found that the EGR is the most important factor in reducing NOx emissions at low and medium loads, whereas fuel injection time is the most important factor in reducing smoke density at high loads. Sathyamoorthi et al. [4] performed a numerical investigation of ZrO_2-coated pistons. The results proved

144

that brake thermal efficiency and indicated thermal efficiency increased by about 5.89% and 11.14%, respectively, when compared to the base engine.

The effectiveness of a thermal barrier coating diesel engine's combustion was investigated by Sathiyagnanam et al., [5]. The cylinder head, valves, and piston crown were coated with about 150:150μm using plasma sparry coating. The experiment was conducted in a thermally barrier-coated diesel engine by blending fuel additive (di isopropyl ether) with neat diesel fuel. It was found that the fuel additives reduce the smoke density of the engine exhaust. The results revealed that the engine's fuel consumption and NOx emissions were lowered while its brake thermal efficiency increased. Shrirao and Pawar [6] tested a diesel engine with a 0.5 mm $3Al_2O_3$ coating and $2SiO_2$ (mullite). At maximum load, the LHR engine with turbocharger demonstrated a 12% rise in exhaust gas temperature, a 22% decrease in CO emissions, and a 28% decrease in HC emissions. The use of kapok oil in diesel engines was tested by Bakthavathsalam [7]. Their approach involves coating piston crowns with Mullite–lanthanum (ML) ceramic composites of different structures to minimize heat rejection. The mixing ratio by volume between ordinary diesel fuel and kapok oil was determined at 20% kapok oil to 80% diesel fuel, and EGR varies between 10% and 30%. The results showed that using ML-coated pistons with biofuel, the brake thermal efficiency reached 29.2%, a 0.2 drop in monoxide pollution, and 39 ppm of engine smoke.

Raut et al. [8] applied a strong magnetic charge obtained from a magnet to the fuel line of a 4-stroke compression ignition diesel engine. The experimental results proved that the permanent magnetic field of 4000 Gauss in the fuel increases the brake thermal efficiency by the accepted range. Jain and Deshmukh [9] used a ferrite magnetic around the fuel line. Magnets in the fuel line improve fuel qualities such as aligning and orienting hydrocarbon molecules improving fuel atomization (better air-fuel mixing). It was found that the MFC improves the mileage of a vehicle by 10% to 40% while reducing harmful carbon monoxide (HC) emissions and other pollutants. Also, prevents diesel engine clogging problems and saves money. Mohammadi et al. [10] completed several experiments on ethanol-diesel mixtures. Particle matters have been reported to reduce with a 100% increase in engine load when the ethanol-diesel blend ratio increases by 20%. The decline in NOx is higher with increased EGR using an ethanol-diesel blend ratio of 20%. The soot level in the exhaust is lower than in base diesel than in diesel fuel. Saravanan et al. [11] described an experimental test on variable speed C.I.E compression ignition using a diesel-ethanol blend. EGR varied over a wide range, and optimization was performed using a double blend. It was found that 10-20% EGR is reasonable to increase the efficiency by 2.32%-6.32% and reduce NO× emissions and engine noise. Yasin et al. [12] investigated the influence of the EGR system, designed for the diesel engine with four cylinders. Moreover, the research also included its effect on bio-diesel fuels and Palm biodiesel. The percentage of NO× was reduced by (5.4%) for diesel and (22% for palm biodiesel).

All the mentioned papers are aimed at the performance and emissions of diesel engines under either a magnetic field or an EGR with a ceramic coating. This paper aims to investigate the impact of thermal barrier coating on diesel engine performance using fueled diesel and biodiesel with the combined influence of EGR and MFC. A coated diesel engine's performance and pollution levels are studied and discussed.

2. Experimental work

The first section covered the experimental stages for coating, such as selecting and preparing samples for coating. In contrast, the second covered the magnetic field setup, the process for creating bio-diesel fuel, the exhaust gas recycling system, and the engine rig's experimental tests. Figure 1 shows the steps of experimental work. This phase was completed at the Malek Ashtar University (Iran-Tehran) Laboratory.
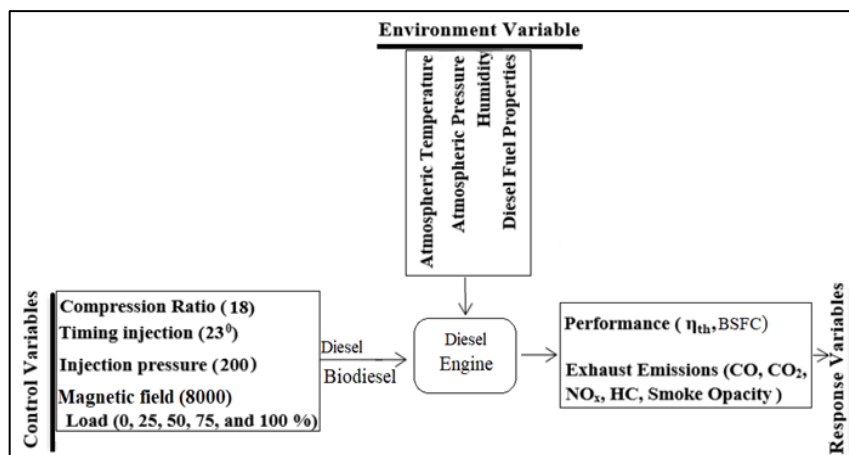

Figure 1: The steps of experimental work

2.1 Coating preparation

2.1.1 Preparation of diesel engine parts

Selecting and preparing spare parts for a diesel engine is step one. During the coating procedure, the method was followed. The normal diesel engine head, including the cylinder, piston, and valves, was machined to eliminate material equivalent to the desired coating thickness while maintaining the same compression ratio. A 500 μm deep groove was cut with a CNC cutter. Because of the complicated design of the cylinder head and piston, CATIA Version 5 had to be utilized for creating specialized

software to aid in the fabrication operations. In the case of the metal face piston, a circle of 500μm thickness was left from total surface area, as illustrated in left photo in Figure 2 (A).

The dimensions checked for cylinder head (W×L×H) (165, 212, and 80 mm), valves face diameters (i.e., valve stem and tip) of both intake and exhausted valves (34.28 mm). The insert photo of Figure 2 (B) shows the setup of coated with nanox (S4007) in a diesel engine.

(A)   **(B)**
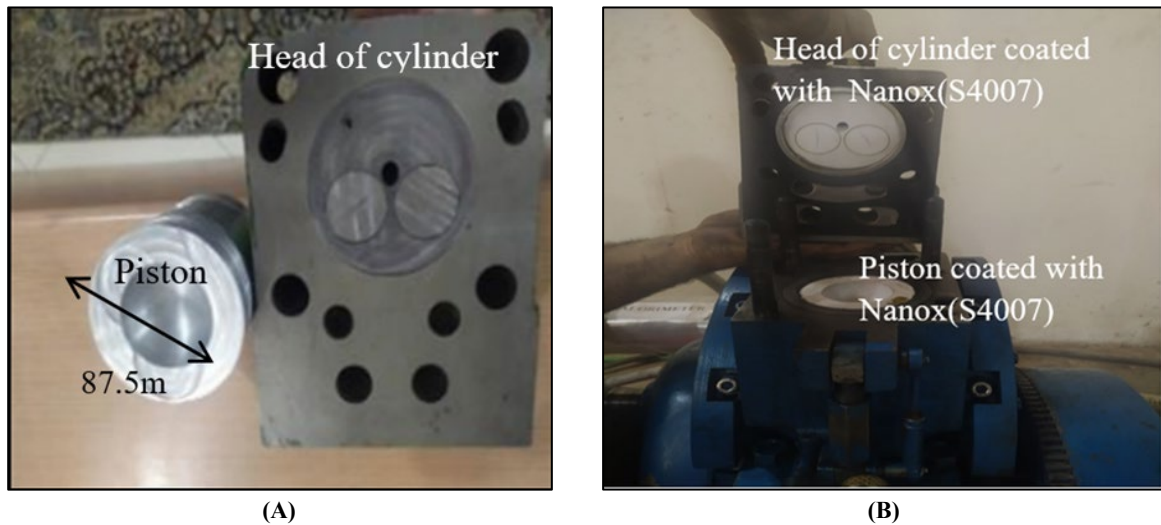
Figure 2: Diesel engine spare parts A- after CNC modeling B- after coating 500 μm with local engine

2.1.2 Preparation of thermal barrier coatings (TBCs)

The nanostructured ZrO$_2$-7 wt was deposited utilizing an Air plasma spray with a Sulzer-Metco F4 (Switzerland) plasma gun. percent Y$_2$O$_3$ (Nanox S4007, Inframat Corp., Farmington, CT) as a feedstock for topcoat. The bond coat was sprayed with micro-structured NiCrAlY powder (AMDRY 962, Sulzer Metco Inc., USA, 56–106 µm) with a nominal composition of (Ni–22 wt-%Cr–10 wt-%Al–1 wt-%Y; AMDRY 962). The bond layer selection was 150 µm in all of the samples tested. The samples were prepared by cutting the combustion chamber parts using a wire cutting machine, where the cutting was done extremely carefully to avoid the production of strains and cracks that can disqualify a sample for future testing. Before testing in a diesel engine, the subsequent tests included FE-SEM, XRD, and utilizing coating properties. In the next portion, the examination process was thoroughly defined and covered.

2.1.3 Air plasma spray (APS)

To increase the mechanical bond of the coating, the surface of the disks was sandblasted with Al$_2$O$_3$ particles of 25-grain mesh before spraying. All specimens were cleaned with acetone to remove any contamination on the surface. Before spraying, the samples were heated to 200 °C in an open environment. Argon and hydrogen plasma gases are used as primary and secondary plasma gases. The unit of gas flow is the normal liter per minute (nlpm), which is often used in Europe, and the reference point is the temperature of the surrounding environment. Table 1 shows the relevant parameters. For a nano-structured coating, spraying characteristics should be chosen so that they can be calculated according to Equation 1 [13]:

$$\text{CPSP} = \frac{VxA}{0.93x\ Q} \tag{1}$$

where A: current in (Ampere), V: is applied voltage (Volt), Q: is a primary argon gas flow rate (normal liter per minute)

2.1.4 The characteristics of the coating

2.1.4.1 Phase analysis

The nanostructured YSZ powder is based on an XRD pattern, shown in Figure 3 (A). The figure demonstrates that granulated nano YSZ powders contain both tetragonal (t) and monoclinic (m) phases. The grain size was calculated using the Scherrer formula, which employed the two high-intensity peaks at low angles, where D is the average diameter of crystallites; β is the broadening of the diffraction line at half maximum intensity, X-ray wavelength, and Bragg angle, and theta is the angle of diffraction. The average crystallite size of the nanostructured YSZ powder is 37-38 nm Equation 2 [13].

$$D = k\lambda / \beta cos\theta \tag{2}$$

Figure 3 (B) shows the X-ray diffraction examination of the bond powder that is used in the present work and for coating both thicknesses (NiCrAlY) and as supplied Ni, Cr-rich (mode), the Ni$_3$Al (phase) highs, as well as a few evidence that AlNi (mode), have all been easily visible.

Table 1: Parameters of Plasma Spraying

Parameter	NiCrAlY	Nanostructured YSZ
Current (A)	600	620
Primary gas, Ar (slpm)	60	42
Secondary gas, H_2 (slpm)	14	10
Carrier gas, Ar (slpm)	2.3	2-4
Powder feed rate (g/min)	40	18
Spray distance (mm)	120	100-120
Traverse speed (rpm)	1	1

(A)   (B)
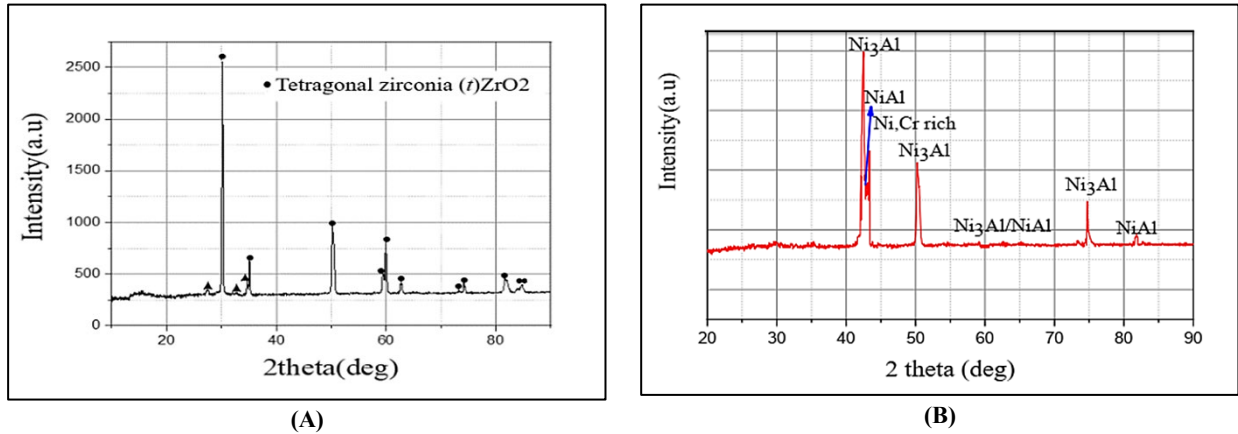
Figure 3: A- XRD pattern for nano nanostructured YSZ powder B- XRD patterns of normal NiCrAlY powders

2.1.4.2 Polished cross-section

Figure 3 depicts the polished sample. The cross-sectional image is related to the substrate as sprayed with a thickness of 500 μm. The nano YSZ (350±50 μm) and NiCrAlY layers of the sample (150±50 μm), a two-layer coating, are clearly separated by a distinct line in the figure. Void and porosity may be spotted all over the ceramic top layer. TBC coating structure shows no fractures or irregularity in the top layer, according to Figure 4. From the NiCrAlY layer to YSZ, the coating pattern gradually changes. Between the YSZ and NiCrAlY layers, a two-phase microstructure of white YSZ and black NiCrAlY can be seen in the microstructure. There are no visible differences between the graded layers.
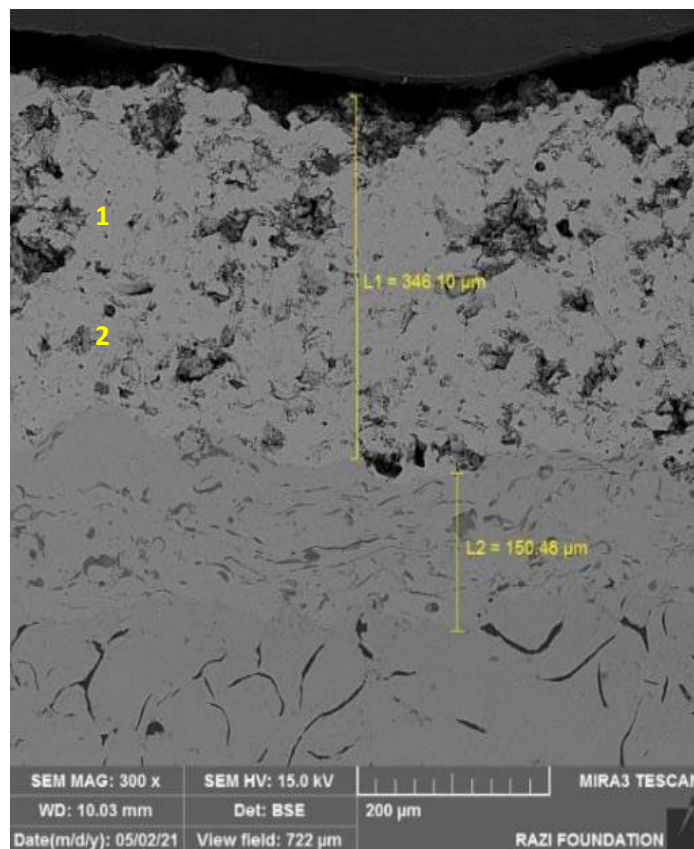
Figure 4: Polished cross sectional 0.5 mm coating cast iron substrate

In the EDS elemental map analysis shown in Figure 5, evaluation relates to points (1) and (2). In contrast to the two-layer system, which exhibits a distinct boundary between the bond and top coat elements, the analysis of the single-layer system presented in Figure 5 (A) demonstrates no such interface. In Figure 5 (B), EDS analyzed the elemental analysis of this cross-sectional view and, as expected, the presence of the Zr element and Y. The presence of Y and Zr in the nano YSZ layers and Ni, Cr, Al, and Y in the bond coatings is plainly visible.
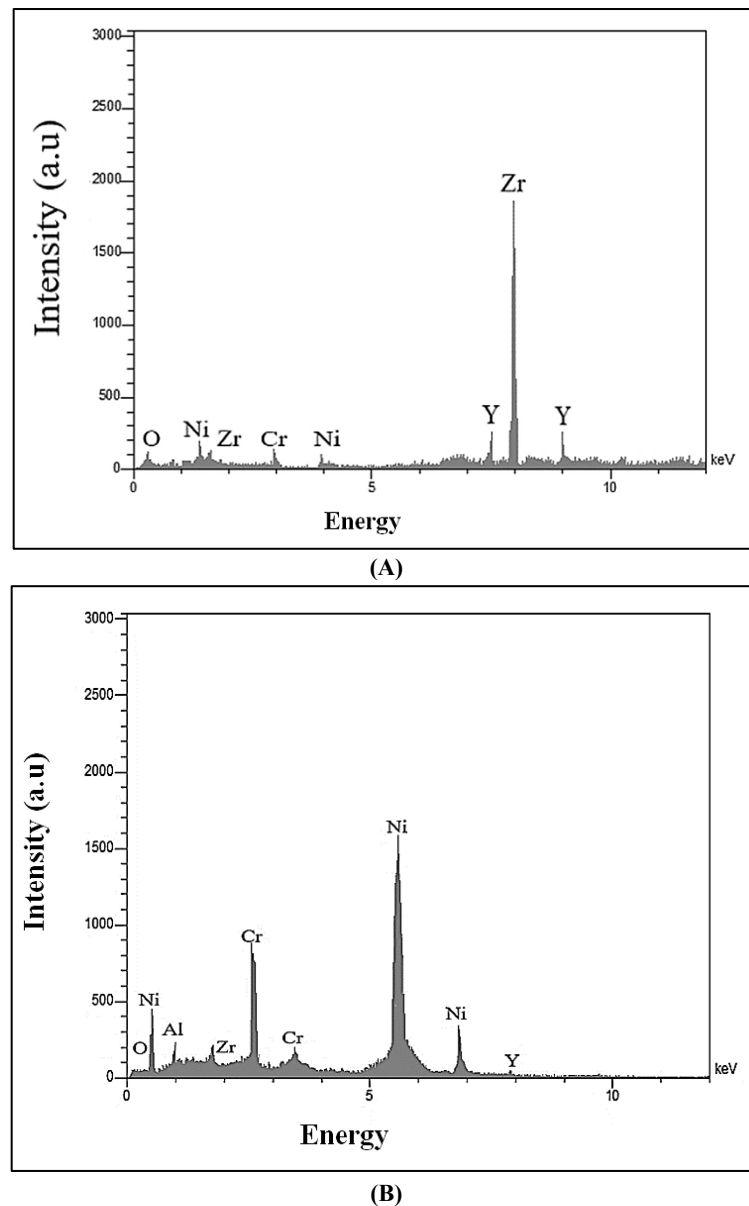

(A)

(B)

Figure 5: A- 500 μm coating EDS analysis point 1 and B- point 2 for Figure 4

2.2 Biofuel preparation

This study used the alkali-catalyzed transesterification process to transform waste cooking oil into an ester. The used cooking oil was heated to 75°C to dilute and remove humidity [14]. Potassium methoxide was produced by dissolving potassium hydroxide in 25% (v/v) methanol 1.5 percent m/m KOH. Methoxide was merged with waste oil that had already been warmed to the reaction temperature of 55°C after being stirred at a mechanical stirrer's optimum speed, as illustrated in Figure 6 (A). Draining and transferring the solution to the separating funnel allowed the reaction to be finished. The analysis of the separation stage in the funnel revealed distinct stratification into two immiscible layers. The denser glycerin phase settled on the bottom, while the less dense biofuel fraction was collected as the upper layer. All methyl ester was repeatedly washed with distilled water until the extra water and methanol were subsequently eliminated by boiling it to 110°C. It was extensively dried using sodium sulfate (Na_2SO_4) [15]. Subsequently, the contaminants were eliminated using premium paper for filtering. Ready-to-use biofuel is depicted in Figure 6 (B), and it was produced as a brilliant yellow substance. All Physicochemical properties of pure diesel and biodiesel blend are listed in Table 2 .
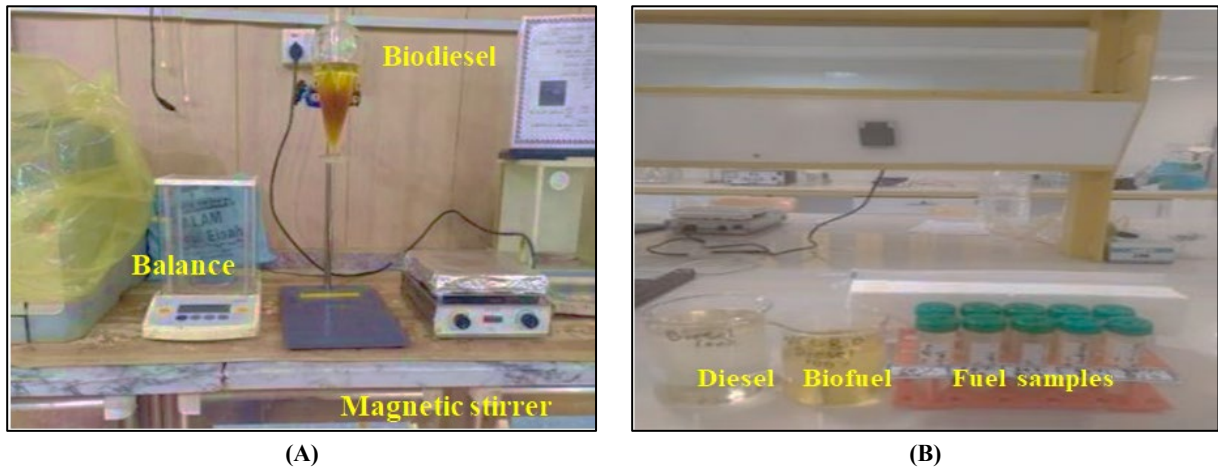
(A)   **(B)**

Figure 6: Biodiesel production A- biodiesel separation and B- fuel samples preparation

Table 2: Physicochemical Properties of pure diesel, biodiesel blend

No	Fuel type	KV@38 (^{o}C) Cst	Density (kg/m^3) @38 °C	Flash point (°C)	CN	LCV (kJ/kg)
1	Diesel	2.57	832	70	51.2	42.35
2	B10	3.2	845	72	51.8	41.20

2.3 Diesel engine magnetic field

The calibrated Gauss meter that was employed to determine the strength of the magnetic fields is depicted in Figure 7 (A). The permanent Neodymium-Iron-Boron magnet that was applied in this study is shown in Figure 7 (B). A magnetic field with an intensity of 1000 Gauss was directed to ionized fuel before it was introduced into the combustion chamber [11].
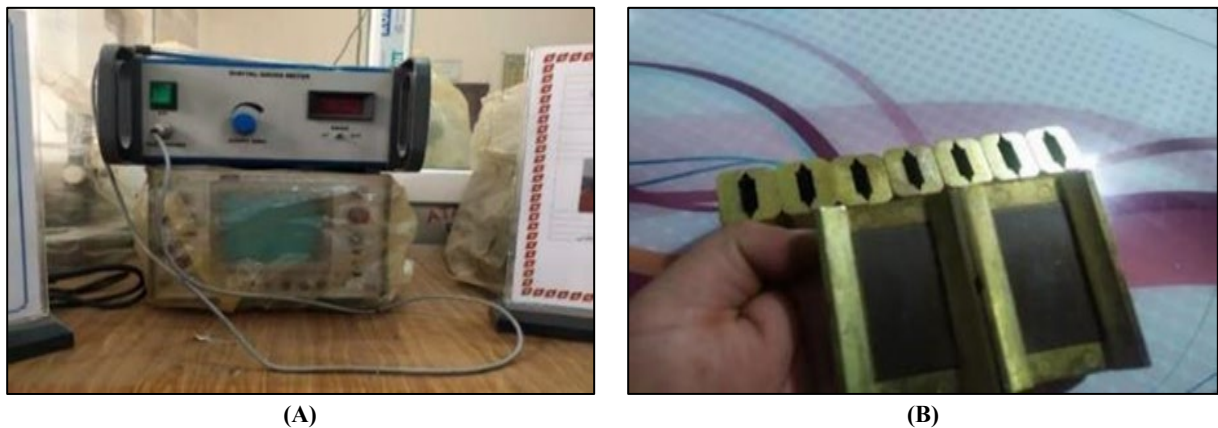

(A)   **(B)**

Figure 7: A- Gauss meter and B- magnetic fuel energizer

2.4 Exhaust Gas Recirculation

Figure 8 (A) shows the EGR parts. The setup used in this work consists of EGR copper and steel pipes, a surge tank, a water inlet port water flow meter, a rotameter, thermocouple arrangements, control valves, and an EGR flow line, while photograph 8B depicts the EGR collection.The experimental engine's exhaust gases were permitted to enter the EGR system. The temperature of the exhaust is decreased to ambient temperature by feeding it through a cooling system and then into the suction manifold. A control valve is used to introduce a regulated rate of flow of engine exhaust and fresh air into the intake port. Equation 3 is used to compute the percent EGR [16,17,18]. All specifications of the EGR system were listed in Table 3.

$$\%EGR = \left[\frac{\text{volume of air without EGR} - \text{volume of air with EGR}}{\text{volume of air without EGR}} \right] x100 \qquad (3)$$

Table 3: Main parts of EGR system

Aluminum pipe length	0.295 m
Copper pipe (RC inner)	0.034 m
Copper pipe (RC outer)	0.036 m
Outer aluminum piper (RA inner)	0.056
Outer aluminum piper (RA outer)	0.058 m
K copper	401 W/m°C
K aluminum	250 W/m°C

Figure 8: A- Diesel engine EGR parts and B-Diesel engine EGR parts after collection

2.5 Diesel engine testing

The engine used in the test featured a variable compression ratio (VCR=12-18) manufactured by Kirloskar (TV1) one cylinder, 4 strokes the engine cylinder volume was (66 cm^3); bore (87.5mm), stroke (110 mm) and running at constant speed 1500rpm. Figure 9 shows the diesel engine testing used in the current work. The rig has an eddy current dynamometer and calorimeter type pipe in the pipe. Additional working characteristics, such as a cooled flow of water of 250 L per hour, are carried out in compliance with the design instructions. The test was carried out at diesel fuel injection timing of 23° bTDC, fuel injection pressure of 200 bar, ambient temperature of 27°C, and engine running speed of 1500 rpm. When experimenting, the engine is driven at idle for approximately 20 minutes. Additionally, this period is long enough for the temperature of the exhaust gases to stabilize. The apparatus used in the experiments is installed in laboratories at the University of Babylon's College of Musayyib Engineering.

2.5.1 Measurement of brake torque

The (C.I. engine) brake torque was measured using an eddy dynamometer. Definition of the eddy current system is listed in Table 4.

Table 4: Specifications of eddy current system

Model	AG-10
Make	SAJ Test Plant Pvt. Ltd
Water inlet	1.6bar
Torque (N. m)	20
Hot coil voltage max.	60
Continuous current Amps.	5
Cold resistance Ohms	9.8
weight	130 kg

Figure 9: Front view of the experimental set up 1-Diesel engine rig test 2- Eddy current dynamometer 3- Control panel 4- Calorimeter 5- Outer surge tank 6- EGR flow meter 7- Temperature recorder 8- Magnetics setup

2.5.2 Fuel consumption

The fuel measurement system for the fuel consumption rate included a fuel tank, a differential pressure transmitter with a range of 0-500 mm WC, a fuel pipe, and a fuel glass tube. Evaluation of fuel consumption and the time it takes to consume a particular weight of fuel was calculated by the employment of the gravimetric method.

2.5.3 Air consumption

An air box was used to measure the amount of air flowing into the engine. The air box with dimensions (35x35x35 cm) has an orifice with a 20 mm diameter. It is connected to a water manometer to measure the difference in the pressure across the orifice see the image in Figure 10 (A).

2.5.4 Measurement of engine speed (RPM)

An inductive pick-up sensor and a digital rpm indicator detect and display the engine speed. The sensor had a 15 V DC power source and a sensing distance of 4-12 mm. It was situated near the engine flywheel, allowing a precise frequency response. A tiny metallic deflector was installed at the TDC location. Figure 10 (B) shows an image of the photoelectric/inductive proximity pickup with a speed indicator marker and a metallic deflector.
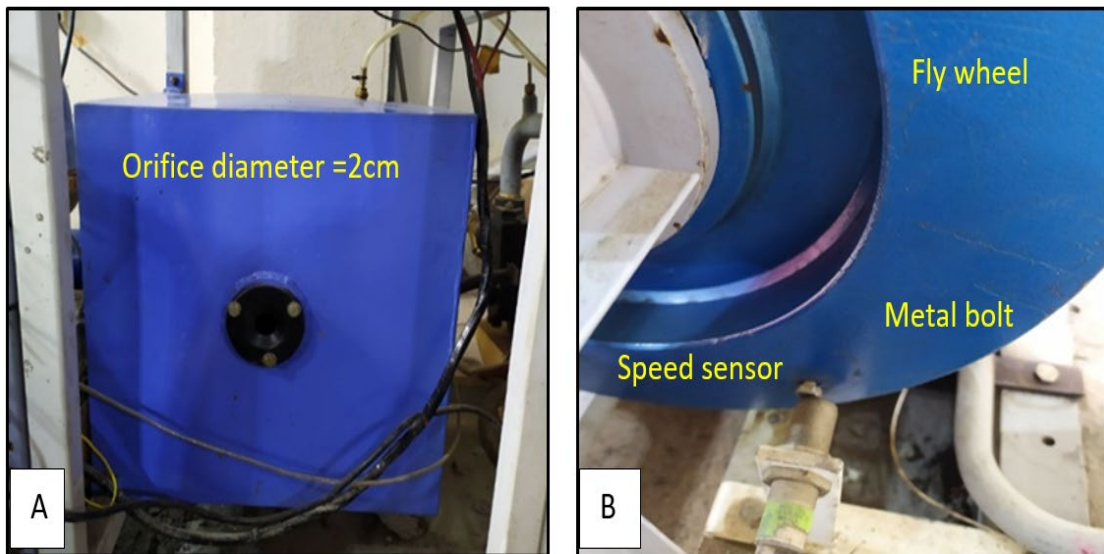

Figure 10: A- air box and B- engine speed sensor setup

2.5.5 Gas analyzer

The exhaust gas analyzer type EGMA (CG-450, Korea) was used to analyze exhaust emissions. The analyzer detects the CO-CO_2-HC and NOx contents.

2.6 Data analysis

The following equations were used in calculating engine performance parameters [11].

1) Engine brake power.

$$BP = \frac{2\pi NT}{60*1000}\tag{4}$$

where N: Engine speed (rpm), and T:Torque (N. m).

2) Brake thermal efficiency is defined as in [15]:

$$BTE\% = \frac{BP}{mf*LCV}\tag{5}$$

where fuel flow rate $\left(\frac{kg}{s}\right)$, LCV: ṁf: fuel flow rate (kg/s), and LCV: fuel calorific value (kJ/kg).

3) The brake specific fuel consumption [16]:

$$BSFC = \frac{mf}{BP}*3600\frac{kg}{kw.hr}\tag{6}$$

4) Air mass flow rate [15]:

$$Actual\ volume\ of\ air = Cd.Aorf.\sqrt{2g\Delta h} \tag{7}$$

where: Cd: orifice coefficient and taken as (0.65), Aorf: Area of orifice plate (m^2), g: gravitational acceleration (m/s^2) and Δh: water manometer reading (m).

5) Uncertainty analysis.

The selection of instruments, conditions, calibration, setting up, notes, measurement, and standardization all contributed to errors and uncertainty in the study's results. The result is determined in an experiment from the primary measurements. The general equation of uncertainty is given by [15]:

$$\frac{U_y}{y} = \left[\sum_{i=1}^{n}\left(\frac{1}{y}\frac{\partial y}{\partial xi}U_{xi}\right)^2\right]^{1/2} \tag{8}$$

Overall uncertainty of the experiment= $\{BP^2 + BTE^2 + BSFC^2 + CO^2 + CO_2{}^2 + UHC^2 + NOx^2\}^{1/2} = 0.1^2 + 0.1^2 + 0.1^2 + 0.1^2 + 0.01^2 + 1^2 + 1^2\}^{1/2} = \pm1.428$.

3. Results and discussion

3.1 Diesel engine performance

The ratio of brake power to fuel consumption and lower heating value (LHV) is defined as brake thermal efficiency. Brake thermal efficiency suggests the combustion system's ability to accept fuel and provides a comparable means of assessing how efficiently the energy in the fuel was converted to mechanical output. Figure 11 (A) the disparity between the normal, 10% WCO +10% EGR +8000G, and adiabatic engines. It is evident that the performance has increased by 13% as a result of the addition of 10% WCO +EGR10% and the usage of the magnetic field, which has improved the fuel's CN. Adding 8000 G magnets, 10% WCO, and 10% EGR rate to insulated engines resulted in a 19.81 percent increase in brake thermal efficiency for the scope of the investigated engine load when compared to diesel fuel. It is clear that permanent magnet fuel with small percentages of recirculating exhaust gases mixes very well with fresh air, leading to complete combustion of the fuel, improved combustion quality, and an increase in overall heat release, as well as thermal barrier coating that prevents heat loss from the walls to the surroundings. The brake thermal efficiency rose because there was less heat transfer from the gas to the walls during combustion or expansion, which caused the walls to get hotter.

Figure 11 (B) portrays the brake specific fuel consumption when the engine ran at a constant speed of 1500 rpm. The magnets were used with bio diesel fuel+ 10% EGR+8000 G, and an LHR engine in the second set of experiments. The curves in the figure show that the BSFC decreases significantly when the engine is operated with just an LHR engine and the combined effect of EGR +8000G. The magnetic field had a direct effect; it affected molecular clustering, resulting in a reduction of fluid viscosity. It also mixed fresh air with 10% EGR in the LHR engine, which resulted in a heat reduction in the heat loss, which ultimately increased the power output and thermal efficiency of the engine, resulting in a reduction in the BSFC. The EGT poorest findings for testing a diesel engine only, while the EGT for external 8000 G polarized+10%EGR, 10% bio fuel with nano-ceramic coated parts were nano-ceramic greater than the engine under normal operating conditions. This is due to the rise in the temperature of the mixture inside the combustion chamber, an increase in the fuel burned per unit time rate, and a decrease in the amount of heat lost through the coating into the cooling system and environment, as portrayed in Figure 12.
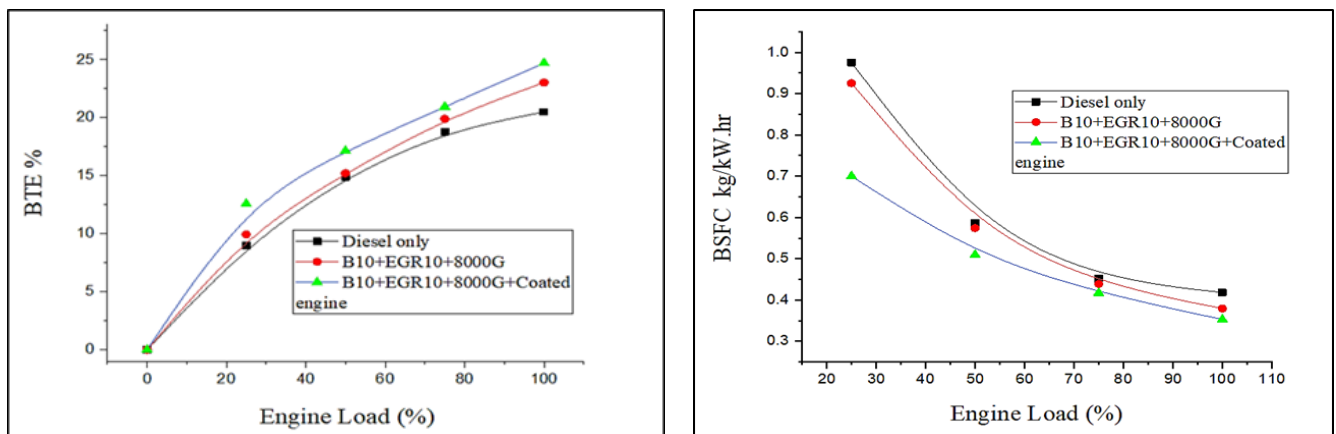

Figure 11: A- variation of BTE with engine loads and B-Variation of BSFC with engine loads
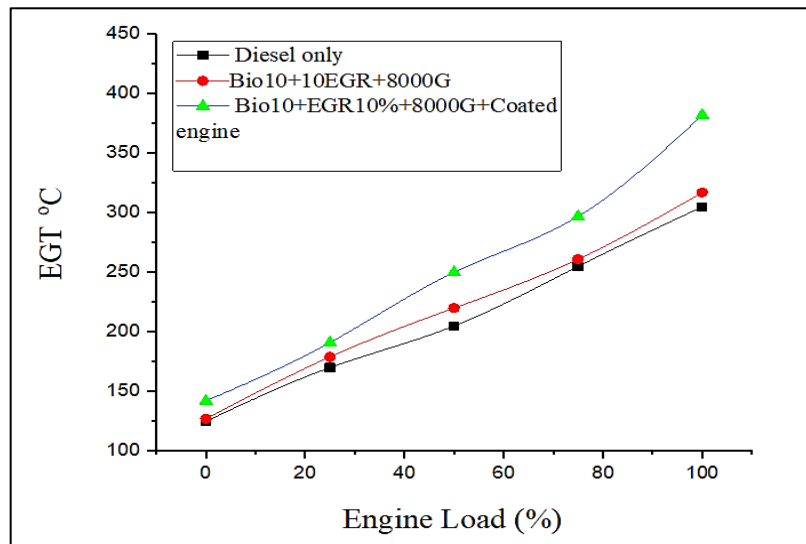
Figure 12: Variation of EGT with engine load

3.2 Diesel engine emissions

Imperfect fuel combustion and a less effective air-fuel mixture are the main contributors to CO emissions. As seen in Figure 13, for the normal and improved engine without coating and the m with coated engine, the carbon monoxide emissions are at their lowest at loads 0, 25, and 50% and begin to grow with a rise in engine load. At coated engines corresponding to 50% and 100% loads, the CO pollutants variation is bordering 0.53 and 0.67 (vol%) and is observed for B10+10EGR+8000 Gauss and diesel fuels, respectively, for uncoated engines. However, 38.8% and a poorer percentage of CO emission are detected once the engine load is improved between 50 and 100% in the case of the B10+10EGR+8000 Gauss fuel 0.5mm coated engine. The reason for the marked decrease is also attributed to the setting of the optimum value of the magnet, as the researchers mentioned, in which the main constituent molecule of the fuel sample is a hydrocarbon (C–H) that has unpaired electron spin moments. A comparable behavior of mon-oxide is practical in the pure diesel case [18].

Figure 14 (A) demonstrates the variant of CO_2 emissions vs. different loads. The normal engine produced the least aunt of CO_2 pollutant for all engine loads (i.e., 0, 25, 50, 75, and 100%). All results indicated that B10 is more suitable for combined impact as biodiesel exposed to the high magnetic field of 8000 Gauss. The presence of extra CO_2 in exhaust emissions shows the fuel was completely burned [19]. Furthermore, an increased CO_2 level of B10 implies practical burning because biofuel's oxygen level increases fuel combustion rates. The result is reinforced by modifications to brake thermal efficiency and BSEC [20]. Figure 14 (B) compares the modernized coated engine to the diesel-powered engine at various engine loads (0, 25 ,50 ,75 and 100%). The diesel-powered engine has the highest pollution levels, as was predicted given that diesel has the lowest CN number. Combined impact operation with the coated exhibited minimum HC emission value of 35 ppm for the same engine load of 100%. Higher levels of HC emission of 54 ppm are observed at uncoated diesel, B10+EGR10+8000 Gauss testing, and engine load of 50%, which was 50 ppm. Increasing HC pollutants have been recorded in uninsulated engines due to fuel quench in the engine's combustion wall. Decreased HC levels were also discovered after an improvement in burning rates and decreased dissociation of molecules during the low heat rejection condition. Moreover, an improvement in oxygen in the combustion chamber is necessary, in addition to using bio-diesel fuel, which is abundant with oxygen, which was considered another source of oxygen in the combustion chamber.

Figure 15 (A) compares a diesel-only and modified engine at various engine loads (0, 25, 50, 75 and 100%). The diesel-only engine has the highest NOx pollution levels. The presence of magnets contributed significantly to reducing fuel viscosity and making it easier to break bonds. The fluctuation of NOx levels with engine loads. The discharged NOx emission was produced near the beginning of the combustion process, where the piston was near the top of its stroke. NOx levels reduction for B10 under combined impacts, with 500µm coated thickness, is adjusted for improved thermal efficiency; this greater reduction of NOx is observed due to coating because zirconia has absorbed nitrogen. Reduction occurs as the intake air is diluted with the EGR 10%. All the above causes led to the reduction of NOx in coated engines. Similarly, According to certain reports, the YSZ coating causes a greater decrease in nitrogen oxides since zirconia absorbs NOx pollutants [21]. As previously mentioned, a higher decline in nitrogen oxides has been found [22] due to coating as a result of nitrogen having been absorbed by zirconia. Many papers were available for thermal barrier coating in diesel engines that experienced a decrease in NOx and also have a good agreement with current work on NOx levels of insulation engines [23], which found similar results in NOx reduction in coated engines. [24] discovered that because of the modified method of combustion, NOx contents were also 10% to 30% fewer.

Yilmaz and Atmanli [25], said that the NOx decreased when using EGR at 20% with a coated engine. The variation in smoke opacity as a function of engine load is seen in Figure 15 (B) for diesel fuel as well as (B10:DF90). The diesel is noted to exhibit the greatest smoke pollutants followed by B10+EGR10+8000 Gauss for uncoated and coated with 500 µm, respectively. The smallest smoke levels indicated for B10-coated engines. The phenomenon may be ascribed to increased combustion chamber temperatures since a thermal barrier is present, exposing the fuel to a high magnetic field intensity of 8000 Gauss. Additional carbon particles participate in the reaction, and the soot precursors are oxidized, which considerably reduces the smoke.
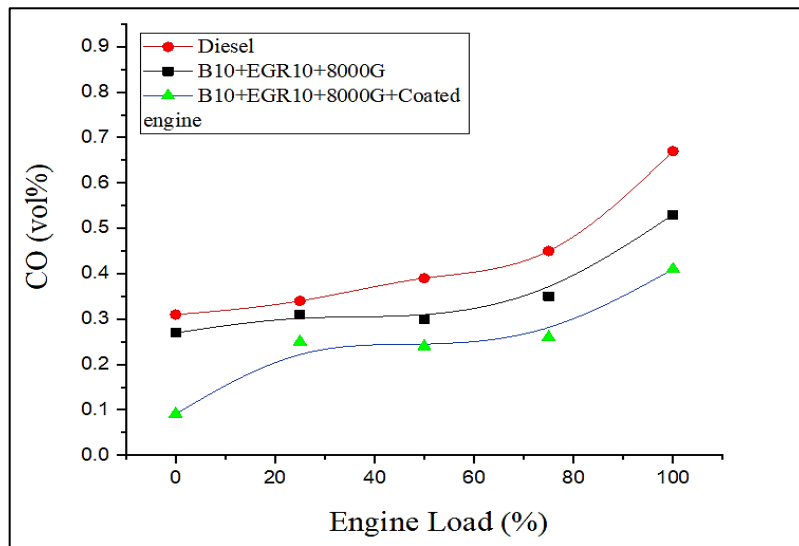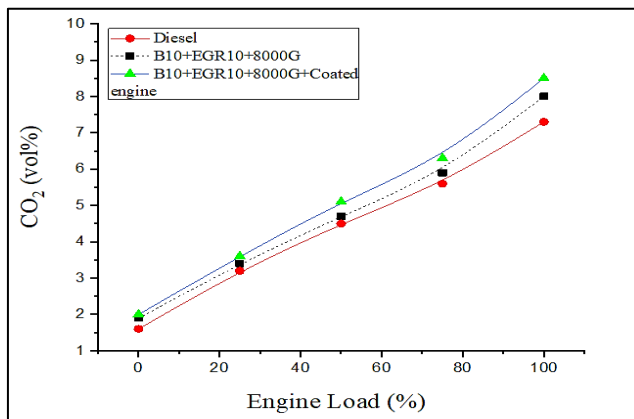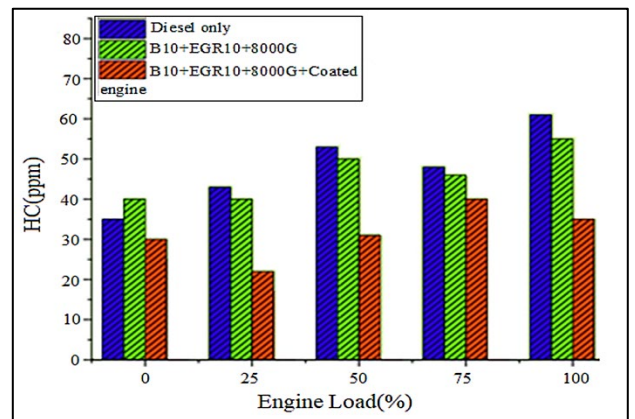
Figure 13: Variation CO emissions with engine loads
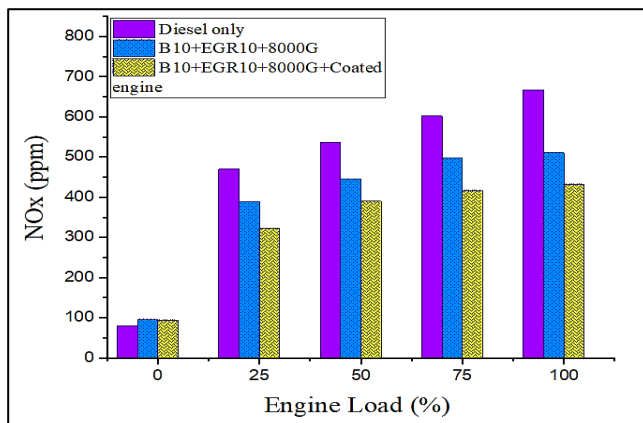

(A)   (B)
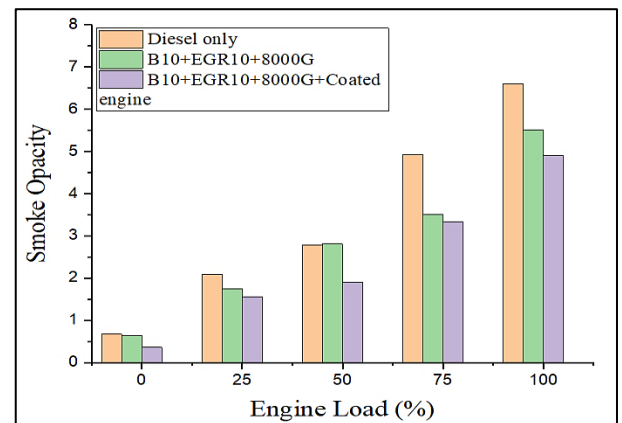
Figure 14: A- variation CO_2 emissions with engine loads and B- variation HC emissions with engine loads

(A)   (B)

Figure 15: A- variation NOx emissions with engine loads and B- variation Smoke Opacity with engine loads

4. Conclusion

The diesel engine parts (head of cylinder, valves, pistons) were coated with a top surface 350 μm nano structure (nano X (S4007)). On the other hand, Amdry 962 powder (Ni-22Cr-10Al-1Y, 52-106 μm) was employed as a conventional bond coat in TBC systems. The following are the main effects of a combined impact of an 8000 Gauss magnetic field + 10% EGR rate + 10% biofuel on a diesel engine with a nano-ceramic coating:

1) The thermal barrier coating (500 µm) nano YSZ and NiCrAlY layers, which is a two-layer coating, are clearly separated by a distinct line. The top layer's thermal barrier coating structure shows no fractures or irregularities.

2) A 10% WCO fuelled LHR C.I engine saw its engine brake thermal efficiency rise by 20% as a result of the addition of a magnetic field and 10% EGR. The combined effect resulted in an 18.1% reduction in brake specific fuel consumption (BSFC). Additionally, when a coated engine was operating at 100% engine load and combined impact, the exhaust gas temperature rose by 25%.

3) When the load is increased from 50% to 100% for the B10+10EGR+8000 Gauss diesel 0.5 mm coated engine, lower CO percent emission figures are noted. There are acceptable increases in emissions were observed in CO_2 levels. Diesel and the B10+EGR10+8000 Gauss un-treatment engine's NOx emission values rise by 49.15 percent and 45 percent, respectively, once the engine load is raised beyond 75%.

4) The peak value of smoke opacity was recorded for pure diesel throughout, followed by B10+EGR10+8000 Gauss for uncoated and coated with 500 µm, respectively. The magnetic field applied to the fuel aids in rearranging fuel atoms in diesel fuel. In addition, integrating the exhaust gas recycling system contributes to reducing the pollutants from the combustion of diesel fuel mixed with biofuel.

Author contributions

Conceptualization, Q. Mahdi, M. Mashkour and I. Mahmoud; formal analysis, Q. Mahdi, M. Mashkour and I. Mahmoud; writing—review and editing, Q. Mahdi, M. Mashkour and I. Mahmoud. All authors have read and agreed to the published version of the manuscript

Funding

Data availability statement

The data that support the findings of this study are available on request from the corresponding author.

Conflicts of interest

The authors declare that there is no conflict of interest.

References

[1] B. Dhinesh, Y. Maria Ambrose Raj, C. Kalaiselvanb, R. KrishnaMoorthy, A numerical and experimental assessment of a coated diesel engine powered by high-performance nano biofuel, Energy Convers. Manag., 171 (201) 815–824. https://doi.org/10.1016/j.enconman.2018.06.039

[2] A. Demirbas, Progress and recent trends in biodiesel fuels, Energy Convers. Manage., 50 (2009) 14-34. https://doi.org/10.1016/j.enconman.2008.09.001

[3] S. Saravanan, G. Nagarajan, and S. Sampath, Combined effect of injection timing, EGR and injection pressure in NOx control of a stationary diesel engine fuelled with crude rice bran oil methyl ester, Fuel, 104 (2013) 409-416. https://doi.org/10.1016/j.fuel.2012.10.038

[4] S. Sathyamoorthi, M. Prabhakaran, and S. M. Abraar, Numerical investigation of ceramic coating on piston crown using Finite Element Analysis, Int. J. Sci. Eng. Appl. Sci., 2 (2016) 258-263.

[5] Sathiyagnanam, A., Saravanan, C., and Dhandapani, S., Effect of thermal-barrier coating plus fuel additive for reducing emission from DI diesel engine Proceedings of the World Congress on Engineering 2010 Vol II WCE 2010, June 30 - July 2, 2010, London, U.K.

[6] P. Shrirao and A. Pawar, Evaluation of performance and emission characteristics of turbocharged diesel engine with mullite as thermal barrier coating, Int. J. Eng. Technol., 3 (2011) 256-262.

[7] S. Bakthavathsalam, R. I. Gounder, and K. Muniappan, The influence of ceramic-coated piston crown, exhaust gas recirculation, compression ratio and engine load on the performance and emission behavior of kapok oil–diesel blend operated diesel engine in comparison with thermal analysis, Environ. Sci. Pollut. Res., 26 (2019) 24772-24794. https://doi.org/10.1007/s11356-019-05678-x

[8] M. S. Raut, S. S. Uparwat, and C. Nagarale, Experimental Inspection by using the Effect of Magnetic Field on the Performance of Diesel Engine, Int. Res. J. Eng. Technol., 4 (2017) 2191-2194.

[9] S. Jain and S. Deshmukh, Experimental investigation of magnetic fuel conditioner (MFC) in IC engine, IOSR J. Eng., 2 (2012) 27-31. https://doi.org/10.9790/3021-02712731

[10] A. Mohammadi, T. Ishiyama, T. Kakuta, and S.-S. Kee, Fuel injection strategy for clean diesel engine using ethanol blended diesel fuel, Technical paper, (2005) 0148-7191. https://doi.org/10.4271/2005-01-1725

[11] P. Saravanan, N. M. Kumar, M. Ettappan, R. Dhanagopal, and J. Vishnupriyan, Effect of exhaust gas re-circulation on performance, emission and combustion characteristics of ethanol-fueled diesel engine, Case Stud. Therm. Eng., 20 (2020)100643. https://doi.org/10.1016/j.csite.2020.100643

[12] M. H. M.Yasin, R. Mamat, A. F. Yusop, D. M. N. D. Idris, T. Yusaf, M. Rasul, et al., Study of a diesel engine performance with exhaust gas recirculation (EGR) system fuelled with palm biodiesel, Energy Procedia, 110 (2017) 26-31. https://doi.org/10.1016/j.egypro.2017.03.100

[13] M. Mashhadi, A. Ashofteh, A. Amadeh, Thermal Shock Behavior of Mixed Composite Top Coat APS TBCs, Ceramics-Silikáty, 62 (2018) 200-209. https://doi.org/10.13168/cs.2018.0013

[14] A. A. A.-h. Qasim, M. A. Mashkour, and I. Al-Namie, The Effect of Ceramic Coating on Performance and Emission of Diesel Engine Operated on Diesel Fuel and Biodiesel Blends, J. Eng., 20 (2014) 91-108.

[15] H. Jumaa and M. A. Mashkour, The Effect of Variable Engine Parameters on Performance and Emissions of DI Diesel Engine Running on Diesel-Biodiesel Blended with Nano Additives, in IOP Conf. Ser.: Mater. Sci. Eng., (2021) 012122. https://doi.org/10.1088/1757-899X/1094/1/012122

[16] Q. Adnan, M. A. Mashkour and I. Mhmood, Combined Impact of EGR Rate and Magnetic Intensity on Performance and Emission of C.I. Engine Operated with Blended Fuel, Int. J. Heat Technol., 40 (2022) 1404-1415. https://doi.org/10.18280/ijht.400607

[17] S. Saravanan, G. Nagarajan, and S. Sampath, Combined effect of injection timing, EGR and injection pressure in NOx control of a stationary diesel engine fuelled with crude rice bran oil methyl ester, Fuel, 104 (2013) 409-416. https://doi.org/10.1080/14786451.2012.743464

[18] P. Singh and S. Chauhan, Feasibility of a new non-edible feedstock in diesel engine: investigation of performance, emission and combustion characteristics, J. Mech. Sci. Technol., 31 (2017) 1979-1986.

[19] R. G. Pereira, C. D. Oliveira, J. L. Oliveira, P. C. P. Oliveira, C. E. Fellows, and O. E. Piamba, Exhaust emissions and electric energy generation in a stationary engine using blends of diesel and soybean biodiesel, Renewable Energy, 32 (2007) 2453- 2460. https://doi.org/10.1016/j.renene.2006.05.007

[20] M. Gumus, Evaluation of hazelnut kernel oil of Turkish origin as alternative fuel in diesel engines, Renewable Energy, 33 (2008) 2448-2457. https://doi.org/10.1016/j.renene.2008.02.005

[21] J. Muthusamy, G. Venkadesan, and U. Krishnavel, Experimental investigation of thermal barrier(8YSZ-TiO2-Al2O3) coated piston used in direct injection compression ignition engine, Therm. Sci., 20(2016) 1189-1196. https://doi.org/10.2298/TSCI16S4189M

[22] N. Karthik, X. G. Xavier, R. Rajasekar, P. G. Bairavan, and S. Dhanseelan, Experimental investigation of performance and emission characteristics of various nano particles with biodiesel blend on di diesel engine, in IOP Conf. Ser.: Mater. Sci. Eng., 197 (2017). https://doi.org/10.1088/1757-899X/197/1/012014

[23] D. W. Dickey, S. Vinyard, and R. Keribar, The effect of insulated combustion chamber surfaces on direct-injected Diesel engine performance, emissions and combustion, SAE Tech. Pap. 1989. https://doi.org/10.4271/890292

[24] E. Buyukkaya and M. Cerit, Thermal analysis of a ceramic coating diesel engine piston using 3-D finite element method, Surf. Coat. Technol., 202 (2007)398-402. https://doi.org/10.1016/j.surfcoat.2007.06.006

[25] N. Yilmaz and A. Atmanli, Experimental assessment of a diesel engine fueled with diesel-biodiesel-1-pentanol blends, Fuel, 191 (2017) 190-197. https://doi.org/10.1016/j.fuel.2016.11.065